

Excited State Features and Dynamics in a Distyrylbenzene-Based Mixed Stack Donor–Acceptor Cocystal with Luminescent Charge Transfer Characteristics

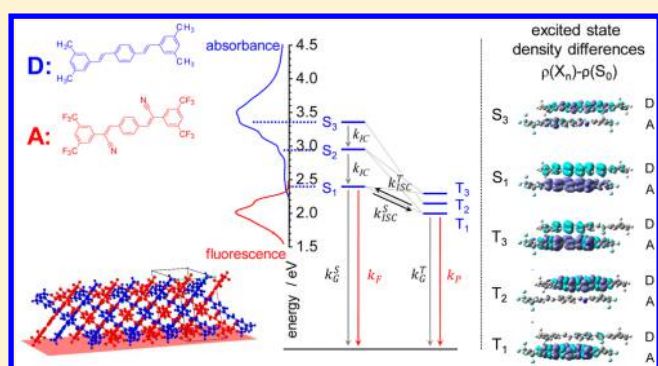
Michael Wykes,^{†,§,⊥} Sang Kyu Park,^{‡,⊥} Santanu Bhattacharyya,^{†,⊥} Shinto Varghese,^{†,||} Ji Eon Kwon,[‡] Dong Ryeol Whang,[‡] Ilhun Cho,[‡] Reinhold Wannemacher,[†] Larry Lüer,[†] Soo Young Park,^{*,‡} and Johannes Gierschner^{*,†}

[†]Madrid Institute for Advanced Studies, IMDEA Nanoscience, C/Faraday 9, Campus Cantoblanco, 28049 Madrid, Spain

[‡]Center for Supramolecular Optoelectronic Materials, Department of Materials Science and Engineering, Seoul National University, ENG 445, Seoul 151-744, Korea

S Supporting Information

ABSTRACT: Combined structural, photophysical, and quantum-chemical studies at the quantum mechanics/molecular mechanics (QM/MM) level precisely reveal the structure–property relationships in a mixed-stack donor–acceptor cocystal, which displays vibronically structured fluorescence, strongly red-shifted against the spectra of the parent donor and acceptor, with high quantum yield despite the pronounced CT character of the emitting state. The study elucidates the reasons for this unusual combination, quantifies the ordering and nature of the collective excited singlet and triplet state manifold, and details the deactivation pathways of the initially created Franck–Condon state.



Organic semiconductors have been intensively investigated through the past decades for applications in (opto)-electronics that cannot be realized by their inorganic counterparts due to a number of advantages in film thickness, flexibility, low weight, transparency, price, and chemical versatility.^{1–3} Within the past few years, increasing efforts have been dedicated toward next-generation multichromophoric materials to achieve novel functionalities by cooperative effects that cannot be achieved by one component alone.^{4–6} However, despite the rapid progress in materials development, the understanding of the resulting electronic, optical, and photophysical properties remains largely qualitative, mainly due to the complex interplay of intra- and intermolecular contributions as well as morphology issues, which control the materials' final optoelectronic properties.^{7–10} Thus, unbiased rational design of complex organic semiconductor materials is one of the key challenges of the field,^{11–13} which can only be developed if structurally well-defined model systems are first properly understood by a combination of advanced photophysical techniques and appropriate computational methods.^{9,10}

We have recently proposed a multichromophoric material, being a single crystalline, densely packed 1:1 D–A mixed-stacked charge-transfer (CT) cocystal based on distyrylbenzene (DSB) derivatives with largely spatially separated frontier molecular orbitals (MOs).¹⁴ Besides its ambipolar charge transport character driven by superexchange mechanism,^{14–16} the crystal promotes an unconventional fluorescence with a

strongly red-shifted spectrum against pure D and A materials due to its pronounced CT character and at the same time a high quantum yield (QY) of more than 30% (see Figure 1). In the present report, we will elucidate the reasons for this unprecedented combination of strong intermolecular CT character and high fluorescence QY, analyze the intermolecular vibronic contributions in the CT emission, and give detailed insight in the excited state manifold that governs the unique photophysics in the system. This requires a correlation of the intra- and intermolecular structural features, as extracted from X-ray analysis, with the excited state (photo)dynamics in the luminescent CT cocystal, done here by a combination of (time-resolved) fluorescence spectroscopy, subpicosecond pump–probe Vis/NIR absorption spectroscopy, and carefully designed QM/MM (quantum mechanics/molecular mechanics) calculations.

Steady state UV–vis absorption spectra were recorded on a nanoparticle (NP) suspension with 1:1 stoichiometry (5×10^{-6} M). In contrast to single crystal (SC) samples, this allows the intrinsic absorption to be measured without being masked by high optical densities.⁹ In fact, the intermolecular arrangement in the NP and SC samples are likely to be similar as suggested by the correspondence in their fluorescence spectra;¹⁴ the latter

Received: July 28, 2015

Accepted: August 31, 2015

Published: August 31, 2015

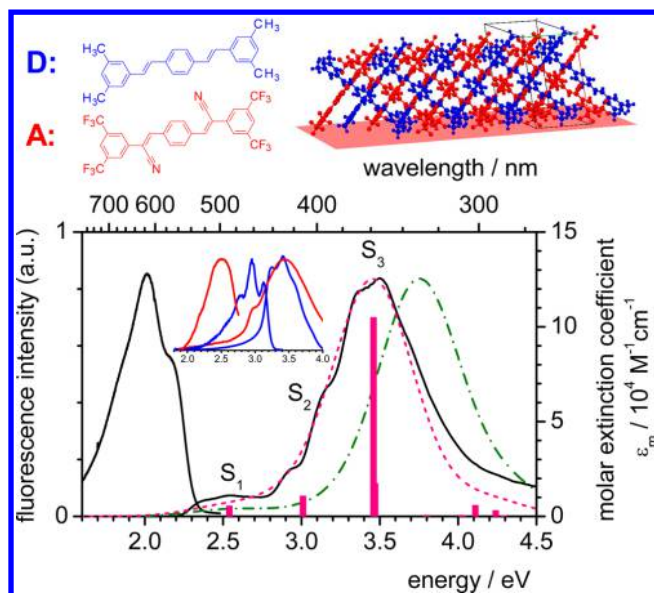


Figure 1. Top: Chemical structure of the donor (D) and acceptor (A) molecules and crystal structure.¹⁴ Bottom: Experimental absorption (right) and fluorescence (left) spectra of the cocrystal nanoparticle suspension (black solid lines). Calculated absorption spectra (TDA- ω B97X-D, pure electronic transitions; Gaussian broadened with $\sigma = 0.25$ eV; normalized intensity); pink dashed line: untuned ($\gamma = 0.20$; shifted by -0.5 eV); green dash-dotted line: IP-tuned ($\gamma = 0.13$). Inset: emission (left) and absorption (right) spectra of donor (blue) and acceptor (red) nanoparticle suspensions.

is indeed a sensitive measure for intermolecular arrangements.¹⁰ The absorption spectrum shows rather plain features with essentially three bright electronic transitions in the visible (see Figure 1). Low lying absorption peaks at 2.38 and 2.55 eV are assigned to the apparent (0–0, 0–1) vibronics of the $S_0 \rightarrow S_1$ transition,¹⁷ where the center of the band (i.e. the vertical transition) coincides approximately with the 0–1 feature; the transition to S_2 consists of vibronics at 2.94 eV (0–0) and 3.12 eV (0–1), and to S_3 of vibronics at 3.36 eV (0–0) and 3.59 eV (0–1). The molar extinction coefficient (and thus oscillator strengths) of S_1 (and S_2) is rather low (i.e. $\epsilon_{m,1} = 1.1 \times 10^4 \text{ M}^{-1}\text{cm}^{-1}$ per D–A pair; Figure 1 and Supporting Information, SI), whereas that of S_3 is intense ($\epsilon_{m,3} = 12.5 \times 10^4 \text{ M}^{-1}\text{cm}^{-1}$). The strong bathochromic shift of the $S_0 \rightarrow S_1$ transition by c. 1 eV against the pure donor and acceptor spectra (located around 3.40 eV)¹⁴ indicates strong CT character, however, with non-negligible oscillator strength ($f = 0.15$; as obtained by integration, see SI), suggesting considerable wave function overlap for the transition. On the other hand, the energetic position and the high extinction coefficient of S_3 suggests a delocalized $\pi\pi^*$ -type transition similar to the pure donor or acceptor molecules.

To verify the assignment, we conducted density functional theory (DFT) studies. However, calculations of larger clusters are computationally expensive, whereas gas-phase dimer calculations do not take into account the effects of crystal packing on geometries. We thus conducted a hybrid QM/MM approach, where the QM system comprised a D–A pair treated at the DFT level, embedded in an MM molecular cluster built according to the known crystal structure,¹⁴ and treated with the Dreiding force field (without charges).¹⁸ This methodology was recently applied for the calculations of DSB clusters, demonstrating that the essential electronic and vibronic features

of the crystal emission spectrum are well reproduced with embedded clusters of modest size.¹⁹ Such localization is even more pronounced for the current D–A system.¹⁴ Indeed, our calculations on larger, symmetric D–A–D, A–D–A, and D–A–D–A–D stacks demonstrate that coupling to shear modes which decreases the lateral D–A offset results in full localization of the emissive exciton onto a single D–A pair, validating our dimer-approach (see SI Figure Q8). Geometry optimization and vibrational normal mode calculations were performed using the ONIOM approach,²⁰ with the MM atoms frozen in their experimental crystal structure positions, and so optimized geometries and normal coordinates were only obtained for the QM region. The S_0 geometry was optimized with the range-separated, dispersion-corrected ω B97X-D functional.²¹ Excited state calculations were performed with the same functional using the Tamm–Dancoff approximation (TDA) to obtain a better estimation of triplet energies, and employing both the untuned range separation parameter (i.e. $\gamma = 0.20$ a.u.) and a system-specific ionization potential (IP) tuned value of $\gamma = 0.13$ to improve the description of excited (in particular CT) states.²² In order to simulate the fluorescence spectrum including vibronic coupling effects,²³ the relaxation of the excited state geometry was also studied with the system-specific gap-tuned (time-dependent; TD) LC-BLYP functional ($\gamma = 0.17$),²⁴ as ω B97X-D calculations predicted large changes in geometry for which the harmonic approximation was found to be inadequate, while S_0 and S_1 geometries optimized with LC-BLYP ($\gamma = 0.17$) provided reasonable agreement with experiments (vide infra). The 6-31G** basis set was used in all cases and all calculations were performed using Gaussian09;²⁵ for further details, see SI.

The calculated TDA-DFT vertical transition energies essentially confirm our state assignment made above, and show an overall good agreement with experiment. The untuned ω B97X-D functional ($\gamma = 0.20$) gave three bright singlet states at 3.05 eV ($f = 0.17$), 3.51 eV ($f = 0.31$) and 3.96 eV ($f = 3.01$), which agrees very well in relative energies and intensities with experiment, if red-shifted by 0.5 eV²⁶ (see pink dashed line in Figure 1). The $S_0 \rightarrow S_1$ transition mainly arises from HOMO (H) to LUMO (L) excitation (93%), where H (L) is exclusively localized in the donor (acceptor) unit. The fact that H-1 and H-2 are relatively close in energy to H (see SI) results in admixing of H-1 \rightarrow L, H-2 \rightarrow L excitations in the configuration interaction (CI) description (see SI), which significantly enlarges the oscillator strength. The $S_0 \rightarrow S_2$ transition reveals partial CT character with main CI contributions by H-1 \rightarrow L, H-2 \rightarrow L and thus enlarged oscillator strength compared to S_1 , while the most intense $S_0 \rightarrow S_3$ transition is mainly donor-localized (H \rightarrow L+1, H \rightarrow L+2). In the IP-tuned variant of the ω B97X-D functional ($\gamma = 0.13$; green dash-dotted line in Figure 1), four relevant singlet states are obtained, with $E(S_1) = 2.56$ eV ($f = 0.11$), $E(S_2) = 3.20$ eV ($f = 0.18$), $E(S_2') = 3.55$ eV ($f = 0.14$), and $E(S_3) = 3.75$ eV ($f = 3.20$) with quite similar CI descriptions compared to the untuned functional, in particular for $S_0 \rightarrow S_1$. The absolute position of S_1 obtained by the tuned functional agrees well with experiment, whereas relative energies and intensities are less well-reproduced compared with the untuned calculations. In order to visualize the rather complex electronic situation in the relevant electronic states, the differences in the excited state densities of holes and electrons for the relevant excited states are shown in the term diagram of Figure 2, in particular highlighting the strong CT character of S_1 and the mainly donor-localized character of S_3 .

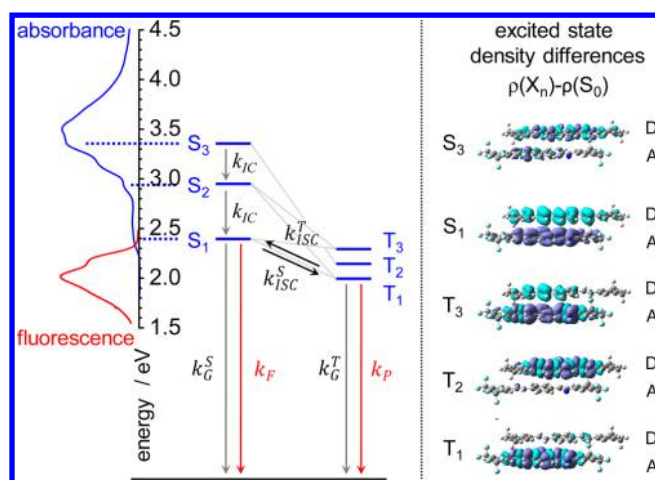


Figure 2. Term diagram for the cocrystal system based on the embedded D–A pair model. Adiabatic energies of the singlet manifold according to the 0–0 bands of the experimental spectrum (left); the S_1 – T_1 gap was estimated from IP-tuned TDA- ω B97X-D calculations. Excited state density differences (light blue = negative, violet = positive) predicted by nontuned TDA- ω B97X-D calculations are given on the right. Rate constants for the S_1 / T_1 deactivation pathways which constitute the TADF process are indicated (fluorescence k_F , phosphorescence k_P , nonradiative deactivation to the ground state from the singlet k_G^S and triplet state k_G^T , intersystem crossing from the singlet k_{ISC}^S and triplet state k_{ISC}^T).

It should be stressed that both methods give a rather large S_1 – S_2 gap, i.e. 0.64 eV (0.46) eV for the (un)tuned variant in good agreement with experiment (0.56 eV), and as well as a large S_1 – S_3 energetic separation (experiment: 0.98 eV), see Figures 1 and 2. This has important consequences for the deactivation within the singlet and triplet manifold; in fact, for internal conversion (IC) from S_3 to S_1 , we found a relatively slow time constant of about 600 fs in the pump–probe measurements (for details see SI). This is clearly evidenced by the delayed buildup of stimulated emission matching the fluorescence spectrum in Figure 1, i.e. a feature specific to the S_1 state.²⁷ The rather slow IC reflects the large interstate separations in the S_n manifold of the cocrystal and possibly also changes in the CT character between these states in agreement with the QM/MM results.

A further consequence of the nature of the frontier orbitals is the state ordering within the triplet manifold, which is reflected in both tuned and untuned TDA-DFT calculations in the same qualitative way: with increasing CT character, the exchange energy (i.e. separation between corresponding singlet and triplet states) becomes smaller, so that the corresponding triplet states of S_1 (strong CT), and S_2 (medium CT) get closer in energy (see Figure 2), generating triplets T_1 , T_3 with more complex CI description compared to the singlets (see SI) and a significantly reduced CT character of T_1 compared to S_1 . As such, the S_1 – T_1 gap is not expected to be as small as in CT states where such mixing does not occur. ΔE_{ST} is predicted to be 0.73 eV by the untuned functional and 0.35 eV by the IP-tuned functional (Figure 2). On the contrary, although the exchange energy of the localized S_3 state is as large as 1.3 (1.4) eV according to the (un)tuned calculations, the large S_1 – S_3 separation still places the corresponding triplet state of S_3 above T_1 , being in fact T_2 as shown in Figure 2 (for details, see Tables Q2, Q3 and Figure Q4 in the SI).

The fluorescence properties of the cocrystal exhibit particular features that arise from the specific D–A arrangement in the cocrystal. Due to the strong CT character of the $S_0 \leftrightarrow S_1$ transition, deep red emission is observed (Figure 1), strongly bathochromically shifted against the pure donor and acceptor materials.¹⁴ Despite the CT character of the emitting state, the emission at room temperature (RT) is vibronically structured (with apparent vibronic bands at 2.18 and 2.02 eV). Cooling the crystal to 1.4 K further sharpens the spectrum (Figure 3);

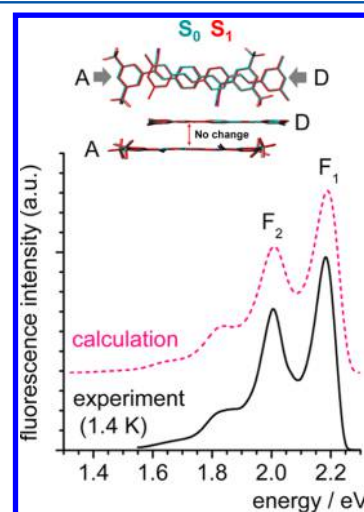


Figure 3. Simulated (pink) and experimental (black) PL spectra of the cocrystal. Inset: superimposed calculated S_0 and S_1 geometries of the donor (D) and acceptor (A). The experiment was recorded on a single crystal at 1.4 K. Simulations were based on the S_1 geometry obtained from TD-LC-BLYP ($\gamma = 0.17$) calculations.

however, the linewidth remains about 0.1 eV, so that details of the vibronic progressions and intercombinations cannot be resolved; contrary to that, e.g., distyrylbenzene single crystals exhibit linewidths smaller than 0.02 eV at 1.4 K.²⁸ The well-resolved features at RT are rather unexpected since emission from CT states like excimers or exciplexes are usually broad and featureless, as a result of large reorganization energies. It should be kept in mind, however, that the actual reorganization will be a sensitive function of the specific geometrical rearrangement upon electronic (de)excitation. For perfect π -stacks of homodimers, i.e. with very small lateral displacements between identical molecules, indeed excimer-like spectra are obtained,^{29,30} arising from a substantial decrease of the interplane separation due to substantial CT contributions.³⁰ This leads to highly efficient coupling of breathing modes which strongly broadens the spectrum.²⁹ In the current case, donor and acceptor are laterally displaced along the long axis (x-slip) by 3.2 Å (see Figure 3). The main intermolecular geometrical change upon $S_0 \rightarrow S_1$ excitation is a reduction of the x-slip by 0.27 Å as calculated by TD-DFT (LC-BLYP; $\gamma = 0.17$), whereas the change in the interplane separation (3.2 Å) is negligible (see Figure 3 and Figure Q6 in the SI). This provokes coupling of shear modes to the electronic transition, which change the lateral displacement, however, with moderate coupling efficiency. The calculated spectrum in the 0 K limit was obtained by a fully atomistic calculation of the vibronics for the embedded dimer (see Figure 3). Remarkably, the calculation not only reproduces the experimentally observed spacing between the apparent vibronics, but in particular the linewidth of the experimental spectrum obtained at 1.4 K, although

only a very small broadening (fwhm 6 meV) was applied.³¹ According to our Franck–Condon analysis, the existence of the unresolved features at 1.4 K indeed arises from vibronic coupling of shear modes as determined by the specific CT character of the cocrystal; the coupling is, however, significantly lower than what is typically observed for the breathing modes in excimers (with Huang–Rhys factors of up to $S = 7$).²⁹

The fluorescence QY of the single crystals was measured as $\Phi_F = 0.31$ – 0.37 depending on crystal size and quality.³² The fluorescence lifetime of the single crystal (as measured by time-correlated single photon counting; TCSPC) is monoexponential with $\tau_F = 17.0$ ns (see SI), which allows the calculation of the radiative and nonradiative rates via $k_F = \Phi_F/\tau_F$ and $k_{nr} = (1 - \Phi_F)/\tau_F$, respectively. Inserting an average of $\Phi_F = 0.35$, we obtain $k_F = 0.021$ ns⁻¹, which is large for CT emission, and arises from the high oscillator strength of the CT state as discussed above; in fact, estimation of the radiative rate via the Strickler–Berg equation gives virtually the same value (see SI). The nonradiative decay rate yields $k_{nr} = 0.038$ ns⁻¹, which is rather low for organic solid state samples,¹⁰ and reflects the dense packing of molecules in the crystal, which restricts large amplitude vibrations. It also indicates that trapping of excitons is not of importance in the current material, which would lead to strongly enhanced nonradiative rates and nonexponential decays.⁹ In principle, such traps can be reached through fast exciton migration, however, the high crystal quality and the long pathway toward the surface of the macro-sized crystals inhibit trapping.⁹ This is very different in nanoparticles of the D–A system with particle sizes of about 50 nm (as determined by dynamic light scattering; see SI); in fact, here the QY is significantly lower ($\Phi_F \approx 0.15$), accompanied by nonexponential lifetimes that are shorter compared to the single crystal (mean lifetime 9.2 ns; see SI). The exciton diffusion length L_D can be estimated from the singlet–singlet annihilation kinetics from femtosecond pump–probe measurements (see SI) giving $L_D \approx 30$ – 40 nm. This is much smaller than the dimension of the single crystal but very similar to the nanoparticle size, rationalizing the high trapping probability in the nanoparticle system.

The nature of the nonradiative decay is ascribed mainly to direct internal conversion (IC) from S_1 to S_0 , whereas intersystem crossing (ISC) to the triplet manifold appears to be a minor pathway since neither phosphorescence was detected, nor delayed fluorescence via thermally activated delayed fluorescence (TADF) or triplet–triplet annihilation (TTA), investigated by careful TCSPC experiments on a microsecond time scale under varying laser flux.³³ The absence of TADF came somewhat as a surprise to us since we initially assumed that the strong intermolecular donor/acceptor frontier MO localization should enhance back-/ISC as in fact observed for intra-^{34,35} and intermolecular CT complexes.^{36–38} The S_1 – T_1 gap in such complexes is mainly driven by the MO energetic offset between the D/A moieties,³⁹ which allows for ISC via second-order spin–orbit coupling. This, however, will sensitively depend on the nature of the accepting triplet state T_x and its energy separation from S_1 . Thus, we ascribe the low efficiency for back-/ISC in the current cocrystal to the strong state mixing within the triplet manifold, which leads to only partial CT character and low energies of the accepting triplet states as revealed from our theoretical analysis drawn above (Figure 2).

In summary, we have conducted a carefully designed in-depth photophysical and quantum-chemical study via a QM/

MM scheme of a densely packed, structurally and electronically well-defined mixed-stack donor–acceptor cocrystal. Together with the available structural information, this allowed us to explore the details of the singlet and triplet state manifolds, and to fully elucidate the electronic nature, vibronic features, and kinetics of the charge transfer (CT) emission. The crystal displays strongly red-shifted fluorescence with high quantum yield despite the pronounced CT character of the emitting state due to a combination of different factors, namely (i) a fairly high oscillator strength of the CT state as driven by configuration interaction, (ii) a low internal conversion rate due to dense packing, and (iii) low trapping probabilities because of the single-crystal quality of the sample, where surface trap states cannot be reached within the singlet exciton lifetime. The QM/MM studies revealed strong state mixing in the triplet manifold, which effectively diminish intersystem crossing despite the strong CT character of the lowest singlet state. Clear signatures of intermolecular vibronic coupling are found in the CT emission and assigned to shear modes of moderate coupling efficiency. Our study thus clearly demonstrates that electronic, optical and photophysical properties of complex organic solid state systems can be indeed successfully elucidated if full structural information via X-ray analysis is combined with (advanced) photophysical techniques and carefully selected, well-justified computational methods.

■ ASSOCIATED CONTENT

Supporting Information

Experimental details, data and analysis of spectroscopic investigations as well as further details and data pertaining to the quantum chemical simulations. The Supporting Information is available free of charge on the ACS Publications website at DOI: 10.1021/acs.jpclett.5b01613.

(PDF)

■ AUTHOR INFORMATION

Corresponding Authors

*E-mail: parksy@snu.ac.kr.

*E-mail: johannes.gierschner@imdea.org.

Present Addresses

[§]PSL Research University, Institut de Recherche de Chimie Paris IRCP, CNRS–Chimie ParisTech, 11 rue Pierre et Marie Curie, F-75005 Paris, France.

^{||}School of Physics and Astronomy, University of St Andrews, Scotland.

Author Contributions

[†]These authors contributed equally to the work.

Notes

The authors declare no competing financial interest.

■ ACKNOWLEDGMENTS

This work was supported by the National Research Foundation of Korea (NRF) through a grant funded by the Korean Government (MSIP; No. 2009-0081571). The work at IMDEA was supported by the Spanish Ministerio de Economía y Competitividad (MINECO; project MultiCrom, Grant No. CTQ2014-58801), by the Comunidad de Madrid (projects Mad2D, Grant No. S2013/MIT-3007, and PhotoCarbon, S2013/MIT-284) and by the Campus of International Excellence (CEI) UAM+CSIC. M.W. thanks the European Commission for his Marie Curie Fellowship (FP7-PEOPLE-

2012-IEF-331795). The spectroscopic and computational work was performed in the context of the European COST Action Nanospectroscopy, MP1302. L.L. acknowledges a Ramón y Cajal fellowship of the MINECO (2010–2015). S.B., S.V., and L.L. acknowledge funding from the EC via the COFUND program AMAROUT. M.W. thanks Ying-Li Niu, Chinese Academy of Sciences, Beijing, for technical assistance concerning use of the MOMAP vibronic coupling code.

REFERENCES

- (1) See, e.g., the thematic reviews in the special issue 'Organic Electronics and Optoelectronics', *Chem. Rev.* **2007**, *107*, 923–1386.
- (2) See, e.g., the thematic reviews in the special issue 'Materials for Electronics', *Chem. Rev.* **2010**, *110*, 1–574.
- (3) See, e.g., the thematic reviews in the special issue 'Organic Photovoltaics', *Acc. Chem. Res.* **2009**, *42*, 1689–1857.
- (4) Yan, D.; Evans, D. G. Molecular Crystalline Materials with Tunable Luminescent Properties: from Polymorphs to Multi-Component Solids. *Mater. Horiz.* **2014**, *1*, 46–57.
- (5) Yan, D. Micro-/Nanostructured Multicomponent Molecular Materials: Design, Assembly, and Functionality. *Chem. - Eur. J.* **2015**, *21*, 4880–4896.
- (6) Kumar, M.; Rao, K. V.; George, S. J. Supramolecular Charge Transfer Nanostructures. *Phys. Chem. Chem. Phys.* **2014**, *16*, 1300–1313.
- (7) Varghese, S.; Das, S. Role of Molecular Packing in Determining Solid-State Optical Properties of π -Conjugated Materials. *J. Phys. Chem. Lett.* **2011**, *2*, 863–873.
- (8) Anthony, S. P. Organic Solid-State Fluorescence: Strategies for Generating Switchable and Tunable Fluorescent Materials. *ChemPlusChem* **2012**, *77*, 518–531.
- (9) Gierschner, J.; Lüer, L.; Milián-Medina, B.; Oelkrug, D.; Egelhaaf, H.-J. Highly Emissive H-Aggregates or Aggregation-Induced Emission Quenching? The Photophysics of All-Trans para-Distyrylbenzene. *J. Phys. Chem. Lett.* **2013**, *4*, 2686–2697.
- (10) Gierschner, J.; Park, S. Y. Luminescent Distyrylbenzenes: Tailoring Molecular Structure and Crystalline Morphology. *J. Mater. Chem. C* **2013**, *1*, 5818–5832.
- (11) Maggini, L.; Bonifazi, D. Hierarchised Luminescent Organic Architectures: Design, Synthesis, Self-Assembly, Self-Organisation and Functions. *Chem. Soc. Rev.* **2012**, *41*, 211–241.
- (12) Chi, Z.; Zhang, X.; Xu, B.; Zhou, X.; Ma, C.; Zhang, Y.; Liu, S.; Xu, J. Recent Advances in Organic Mechanofluorochromic Materials. *Chem. Soc. Rev.* **2012**, *41*, 3878–3896.
- (13) Zhu, L.; Zhao, Y. Cyanostilbene-Based Intelligent Organic Optoelectronic Materials. *J. Mater. Chem. C* **2013**, *1*, 1059–1065.
- (14) Park, S. K.; Varghese, S.; Kim, J. H.; Yoon, S.-J.; Kwon, O. K.; An, B.-K.; Gierschner, J.; Park, S. Y. Tailor-made Highly Luminescent and Ambipolar Transporting Organic Mixed Stacked Charge-Transfer Crystals: an Isometric Donor-Acceptor Approach. *J. Am. Chem. Soc.* **2013**, *135*, 4757–4764.
- (15) Zhu, L.; Yi, Y.; Li, Y.; Kim, E.-G.; Coropceanu, V.; Brédas, J.-L. Prediction of Remarkable Ambipolar Charge-Transport Characteristics in Organic Mixed-Stack Charge-Transfer Crystals. *J. Am. Chem. Soc.* **2012**, *134*, 2340–2347.
- (16) Geng, H.; Zheng, X.; Shuai, Z.; Zhu, L.; Yi, Y. Understanding the Charge Transport and Polarities in Organic Donor–Acceptor Mixed-Stack Crystals: Molecular Insights from the Super-Exchange Couplings. *Adv. Mater.* **2015**, *27*, 1443–1439.
- (17) The apparent vibronics do not belong to one specific normal mode, but result from convolution of all normal modes that couple to the electronic excitation; thermal broadening gives rise to one 'apparent mode' which can be usually fitted with one Franck-Condon progression; for details see Gierschner, J.; Mack, H.-G.; Lüer, L.; Oelkrug, D. Fluorescence and Absorption Spectra of Oligophenylenevinyls: Vibronic Coupling, Band Shapes, and Solvatochromism. *J. Chem. Phys.* **2002**, *116*, 8596–8609.
- (18) Mayo, S. L.; Olafson, B. D.; Goddard, W. A. DREIDING: A Generic Force Field for Molecular Simulations. *J. Phys. Chem.* **1990**, *94*, 8897–8909.
- (19) Wykes, M.; Parambil Mangattu, R.; Beljonne, D.; Gierschner, J. Vibronic Coupling in Molecular Crystals: a Franck-Condon Herzberg-Teller Model of H-aggregate Fluorescence Based on Quantum Chemical Cluster Calculations. *J. Chem. Phys.* **2015**, DOI: 10.1063/1.4930606.
- (20) Dapprich, S.; Komáromi, I.; Byun, K. S.; Morokuma, K.; Frisch, M. J. A new ONIOM Implementation in Gaussian98. Part I. The Calculation of Energies, Gradients, Vibrational Frequencies and Electric Field Derivatives. *J. Mol. Struct.: THEOCHEM* **1999**, *461–462*, 1–21.
- (21) Chai, J.-D.; Head-Gordon, M. Long-Range Corrected Hybrid Density Functionals with Damped Atom–Atom Dispersion Corrections. *Phys. Chem. Chem. Phys.* **2008**, *10*, 6615–6620.
- (22) Körzdörfer, T.; Brédas, J.-L. Organic Electronic Materials: Recent Advances in the DFT Description of the Ground and Excited States Using Tuned Range-Separated Hybrid Functionals. *Acc. Chem. Res.* **2014**, *47*, 3284–3291.
- (23) Niu, Y.; Peng, Q.; Deng, C.; Gao, X.; Shuai, Z. Theory of Excited State Decays and Optical Spectra: Application to Polyatomic Molecules. *J. Phys. Chem. A* **2010**, *114*, 7817–7831.
- (24) Foster, M. E.; Wong, B. M. Nonempirically Tuned Range-Separated DFT Accurately Predicts Both Fundamental and Excitation Gaps in DNA and RNA Nucleobases. *J. Chem. Theory Comput.* **2012**, *8*, 2682–2687.
- (25) Frisch, M. J.; Trucks, G. W.; Schlegel, H. B.; Scuseria, G. E.; Robb, M. A.; Cheeseman, J. R.; Scalmani, G.; Barone, V.; Mennucci, B.; Petersson, G. A. et al. *Gaussian 09*, revision D.01; Gaussian, Inc.: Wallingford, CT, 2009.
- (26) The calculated molar extinction coefficient is $\epsilon_m = 16.4 \cdot 10^4 \text{ M}^{-1} \text{ cm}^{-1}$; i.e. 30% higher in experiment. Although this is likely to be due to the incorrect estimation by experiment, it might be also due to the reduction of the experimentally observed ϵ_m occurring in NPs by size effects as discussed in ref 7.
- (27) Maiuri, M.; Polli, D.; Brida, D.; Lüer, L.; LaFountain, A. M.; Fuciman, M.; Cogdell, R. J.; Frank, H. A.; Cerullo, G. Solvent-Dependent Activation of Intermediate Excited States in the Energy Relaxation Pathways of Spheroidene. *Phys. Chem. Chem. Phys.* **2012**, *14*, 6312–6319.
- (28) Wu, C. C.; Korovyanko, O. J.; DeLong, M. C.; Vardeny, Z. V.; Ferraris, J. P. Optical Studies of Distyrylbenzene Single Crystals. *Synth. Met.* **2003**, *139*, 735–738.
- (29) Gierschner, J.; Mack, H.-G.; Oelkrug, D.; Waldner, I.; Rau, H. Modeling of the Optical Properties of Cofacial Chromophore Pairs: Stilbenophane. *J. Phys. Chem. A* **2004**, *108*, 257–263.
- (30) Gierschner, J.; Ehni, M.; Egelhaaf, H.-J.; Milián Medina, B.; Beljonne, D.; Benmansour, H.; Bazan, G. C. Solid State Optical Properties of Linear Polyconjugated Molecules: π -Stack contra Herringbone. *J. Chem. Phys.* **2005**, *123*, 144914.
- (31) The strength of the vibronic coupling might be somewhat underestimated by the calculations, which could partly explain the small differences in intensity of the first apparent vibronic band (F_1 , at 2.18 eV) between experiment and calculation; in fact, artificially augmenting the change in geometry decreases the relative intensity F_1/F_2 (however, at the same time broadens the spectrum; see SI). This might suggest that the rigidity of the crystal environment is overestimated by our simulations (in which this environment was fixed). Indeed it has previously been shown that including or neglecting environmental flexibility can have a significant impact on the excited state reorganization of an embedded molecule (see ref 40). On the other hand, the difference between experiment and calculation might also arise from reabsorption in the experimental spectrum, which cannot be completely avoided because of the high optical density of the single crystal.
- (32) The NP suspensions gave somewhat lower values for the two fluorescent lifetime components (see SI) and for the QY ($\Phi_F = 0.14$ –

0.15), which we attribute to enhanced trapping; for a discussion, see ref 9.

(33) We stress that the identification of TADF in a microsecond TCSPC experiment is a sensitive issue since the relative amplitude of the delayed component might be 3 orders of magnitude lower than the prompt one. For this reason, a critical assessment of the experimental results with respect to artifacts is indispensable. In fact, independent measurements on different TCSPC setups and at very low emission intensities were performed.

(34) Tao, Y.; Yuan, K.; Chen, T.; Xu, P.; Li, H.; Chen, R.; Zheng, C.; Zhang, L.; Huang, W. Thermally Activated Delayed Fluorescence Materials Towards the Breakthrough of Organoelectronics. *Adv. Mater.* **2014**, *26*, 7931–7958.

(35) Adachi, C. Third-generation Organic Electroluminescence Materials. *Jpn. J. Appl. Phys.* **2014**, *53*, 060101.

(36) Prochorow, J.; Kozankiewicz, B. Delayed Fluorescence of Charge-Transfer Crystals. Triplet-Triplet Annihilation vs. Thermal Activation of Excitons. *J. Lumin.* **1988**, *40-41*, 280–281.

(37) Kozankiewicz, B. Excitonic Energy Transfer in Mixed-stack Charge Transfer Crystals. *Adv. Mater. Opt. Electron.* **1996**, *6*, 371–374.

(38) Kozankiewicz, B. Electronic Energy Transfer in the Charge-Transfer Crystal of 2,3-Dimethylnaphthalene-tetracyanobenzene. *J. Lumin.* **1997**, *71*, 37–46.

(39) Milián-Medina, B.; Gierschner, J. Computational Design of Low Singlet-Triplet Gap All-Organic Molecules for OLED Application. *Org. Electron.* **2012**, *13*, 985–991.

(40) Srinivasan, G.; Villanueva-Garibay, J.; Müller, K.; Oelkrug, D.; Milian Medina, B.; Beljonne, D.; Cornil, J.; Wykes, M.; Viani, L.; Gierschner, J.; et al. Dynamics of Guest Molecules in PHTP Inclusion Compounds as Probed by Solid-State NMR and Fluorescence Spectroscopy. *Phys. Chem. Chem. Phys.* **2009**, *11*, 4996–5009.